Journal of Alloys and Compounds 797 (2019) 262–268

Contents lists available at ScienceDirect

Journal of Alloys and Compounds

journal homepage: http://www.elsevier.com/locate/jalcom

Enhancing thermal properties of few-layer boron nitride by high-*k* Al_2O_3 capping layer

Yuxuan Chen [a, b], Kuilong Li [c], Zhiwen Li [d], Shengqun Hu [d], Xiaojuan Sun [a], Zhiming Shi [a], Xinke Liu [a, b, *], Dabing Li [a, b, **]

[a] State Key Laboratory of Luminescence and Applications, Changchun Institute of Optics, Fine Mechanics and Physics, Chinese Academy of Sciences, Changchun, 130033, People's Republic of China
[b] Center of Materials Science and Optoelectronics Engineering, University of Chinese Academy of Sciences, Beijing 100049, People's Republic of China
[c] School of Electronic and Information Engineering (Department of Physics), Qilu University of Technology (Shandong Academy of Sciences), Jinan, 250353, People's Republic of China
[d] College of Materials Science and Engineering, Shenzhen University, Shenzhen, 518060, People's Republic of China

ARTICLE INFO

Article history:
Received 13 March 2019
Received in revised form
3 May 2019
Accepted 9 May 2019
Available online 14 May 2019

Keywords:
Boron nitride
Thermal conductivity
Raman spectroscopy

ABSTRACT

Atomically thin boron nitride (BN) film has attracted increasing attention among two-dimensional materials for the potential application in electronics devices. The thermal properties of few-layer BN nanosheets (~2.27 nm) on SiO_2/Si substrates have been investigated without and with high-*k* Al_2O_3 capping layer, using the temperature-dependent and polarized-laser power-dependent Raman spectroscopy measurements. Due to the effect of Al_2O_3 capping layer, Raman spectrum illustrates the blue-shift of frequency from 1364.9 cm^{-1} to 1367.9 cm^{-1}, and the first order temperature coefficient for E_{2g} mode of BN layers increases from −0.02243 cm^{-1}/K to −0.06544 cm^{-1}/K. Furthermore, the room-temperature thermal conductivity of BN with Al_2O_3 capping layer is found to be 332.57 W/mK, which is much larger than that of BN without Al_2O_3 capping layer (~94.51 W/mK). The enhancement is attributed to the interface charges and compressive stress at the interface between BN and Al_2O_3 capping layer, which has been clarified by the first principle calculations. This work is aimed at expanding the applications of BN materials and improving the performances of BN-based devices in thermal properties.

1. Introduction

Atomically thin hexagonal boron nitride (hBN) nanosheets, with similar structure to graphene, have attracted increasing attention among two-dimensional (2D) materials, exerting preferable mechanical, thermal, chemical and optical properties [1,2]. BN is isomorphic to carbon in various kinds of crystalline structures, including zero-dimensional nanospheres, one-dimensional nanotubes, two-dimensional nanosheets and three-dimensional bulk structures. It consists of boron and nitrogen atoms alternately arranged in a hexagonal ring via sp^2 hybridization. In contrast to excellent electrical conductivity of graphene, BN is equipped with a wide band gap (~5.9 eV) [3,4], referred as an insulator. Subsequently, hBN has been proven to be an ideal gate dielectric or substrate in graphene-based devices or other devices due to its atomically flat surface, scarceness of dangling-bond, and the close lattice matching (~1.7%) between BN and graphene [5–9]. Improvement over an order of magnitude in electron transport and carrier mobility, together with various unique quantum phenomena can be observed in vertical graphene/hBN heterostructure [10,11]. Besides, the wide direct band gap of monolayer BN brings potential application of the ultraviolet lasing materials in photodetector (wavelength of 210 nm) [2,12,13], as well as, in the capacity of prototypical infrared-phononic material, hBN ribbons are made into hyperbolic phonon polaritons (HPhPs) Fabry–Pérot resonators to detect small amounts of organic molecules [14]. Meanwhile, hBN was also reported as micro/nanoscale thermal management of high-power devices behind graphene [15,16], which means both of them can successfully spread heat to reduce the temperature at hotspot [16]. However, few-layer graphene (FLG) was limited to

* Corresponding author. State Key Laboratory of Luminescence and Applications, Changchun Institute of Optics, Fine Mechanics and Physics, Chinese Academy of Sciences, Changchun, 130033, People's Republic of China.
** Corresponding author. State Key Laboratory of Luminescence and Applications, Changchun Institute of Optics, Fine Mechanics and Physics, Chinese Academy of Sciences, Changchun, 130033, People's Republic of China.
E-mail addresses: liuxinke@ciomp.ac.cn (X. Liu), lidb@ciomp.ac.cn (D. Li).

https://doi.org/10.1016/j.jallcom.2019.05.115
0925-8388/

cover the drain and unable to connect to the channel directly, owing to that its outstanding electrical conductivity may easily cause breakdown and short-circuit accident, so it is comparably important to understand the properties and application of BN as a thermal management component in electrical devices. The room-temperature thermal conductivity of bulk hBN can reach ~400 W/mK, as well as, the enhanced in-plane thermal conductivity of monolayer hBN is theoretically expected to be more than 600 W/mK, but experimentally measured to be only 100–270 W/mK [17–19]. The high thermal conductivity makes BN as fillers of polymeric composites [20] or promising heat-spreading layers in transistors, which often work at temperature over 100 °C. So, without the process of heat dissipation, the accumulated energy may deactivate microelectronic devices. Nowadays, with the decrease in feature sizes in micro/nano-electronic devices, the density of dissipation power has significantly increased. As a result, efficient heat conduction occupies an important place as a vital design characteristic in integrated circuits. In other words, thermal dissipation is a nonnegligible limiting factor to further device miniaturization. It is said that Si and some insulators, such as Si_3N_4 and SiO_2, used in traditional devices behave unsatisfactory performance in nano-scale thermal conductivity. So, research of BN is encouraged by the potential of thermal management, with a combination of its lower electrical conductivity and higher thermal conductivity. Furthermore, this work will also extend the application of BN as the thermal management in optoelectronics and photonics fields and lead the trend for other two-dimensional layer materials in thermal application.

In this work, we report the thermal conduction properties of atomically thin BN nanosheets on SiO_2/Si substrates without and with a ~5 nm Al_2O_3 capping layer. The Raman spectrum illustrates the blue-shift of frequency for the BN sample with Al_2O_3 capping layer. Meanwhile, the temperature-dependent Raman spectroscopy shows the increase of the thermal coefficient, and the polarized-laser power-dependent Raman spectroscopy shows the improvement of the thermal conductivity. Herein, we demonstrate a proof-of-concept for those changes and the first principle calculations have been carried out to explore the phenomena, which reveal that the interface charges and compressive strain at Al_2O_3/BN heterojunction enhance the thermal conductivity. This thermal property improvement introduced by the additional oxide will extend the applications and enhance the performances of BN-related devices profoundly.

2. Experiment details

The atomically thin BN nanosheets were mechanically exfoliated from monocrystalline BN bulks by scotch tape and then transferred onto the silicon substrates covered with 300 nm-thick SiO_2 layer, as shown in Fig. 1 (a). Later the samples were deposited with 5 nm-thick Al_2O_3 capping layer, which was grown using trimethylaluminum (TMA1) and H_2O as precursors at 300 °C by atomic layer deposition (ALD) method [21]. Atomic force microscopy (AFM) images of the samples were analyzed by a Bruker Dimension ICON Atomic Force Microscope operating in tapping mode. In addition, temperature-dependent Raman measurements ranging from room temperature (300 K) to 500 K were carried out and 5 min were waited for thermal stabilization at each measured

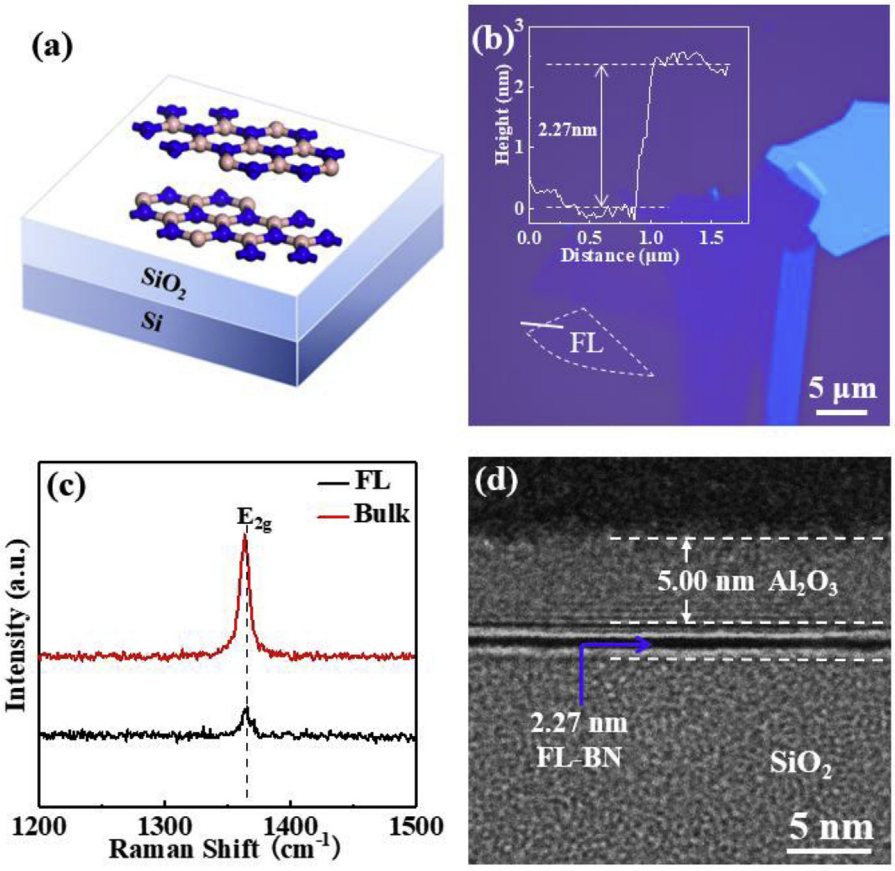

Fig. 1. (a) Atomic structure model schematic diagram of few-layer BN on SiO_2/Si. (b) Optical microscope image of FLBN and the corresponding height profile shown in the inset. (c) Raman spectra of BN bulk and few-layer samples before and after mechanical exfoliation, and (d) transmission electron microscopy (TEM) image of FLBN with Al_2O_3 after ALD.

temperature point. Laser-dependent Raman measurements below 2.5 mW were carried out in case to introduce Raman shifts by local laser heating. All the Raman studies were carried out with a confocal micro-Raman spectrometer setup with a solid-state green laser at 514 nm excitation wavelength.

3. Results and discussion

The atomically thin BN nanosheets mechanically exfoliated from monocrystalline BN bulks on SiO_2(300 nm)/Si substrates were situated and observed with optical microscope. Fig. 1 (b) shows the flat transferred-nanosheets with distinct boundary and the height profile across the edge of the BN sample is in the inset. It seems that the color contrast between this thinnest area and the SiO_2/Si substrates is nearly undetectable by the human eye. Because of the wide band gap, atomically thin BN nanosheets exhibit little optical contrast, even if we have used SiO_2 on Si substrate to enhance the interference. It is reported that BN layers show a white-light contrast of <1.5% with 300 nm SiO_2 [22]. Furthermore, we determined the regions of the few-layer nanosheets by AFM measurement and the thickness of the thinnest BN layers visible to the naked eyes is about 2.27 nm. According to the previous research [23], the sample seems a stack consisted of 4 or 5 layers so that we define it as few-layer boron nitride (FLBN). It is seldom to obtain such thin 2D materials via exfoliate method and FLBN can make most use of the thickness advantage, since its wide indirect band gap can safely protect itself from breakdown. In fact, for hBN, the in-plane thermal conductivity is much higher than the out-plane thermal conductivity so that we consider to fully utilize the thermal property by means of adopting boron nitride in few layers.

Raman spectroscopy is a well-known technique to characterize the 2D-materials [24–26], for instance of graphene and MoS_2 [27,28], for further understanding of the fine structure and properties, such as the nature of atomic bonds, thermal expansion, specific heat, and thermal conductivity. However, the Raman spectrum of BN contains only one peak without 2D band due to the lack of Kohn anomaly [29], which is limited to explain its properties like graphene or other 2D-materials, with their crystallinity, dimensions, doping and so on. Actually, it is not easy to isolate such large-scale atomically thin BN layers by micro-mechanical exfoliation of high-quality hBN, for difficulty of detecting Raman signals originated from FLBN. Fig. 1 (c) contrastively shows the typical Raman spectra of original bulk and exfoliated thin films of BN both at room temperature. The single Raman G band of BN bulk, corresponding to the E_{2g} vibration mode in hBN, is located at 1363.74 cm^{-1}. In contrast with bulk BN, the few-layer BN obviously shows an upshifted G band reflected in the Raman frequency at 1365.76 cm^{-1}, due to the stronger in-plane strain and weaker interaction of layers. The shift direction is in accord with the previous research [29]. Therefore, it suggests that Raman peak position of BN is related with thickness of the material, as well as, the blue-shift of frequency corresponding to thinner sample mainly arises from strain introduced by the uneven surface of the substrate, which gives rise to different degrees of corrugation. As shown in Fig. 1 (d), transmission electron microscope (TEM) image shows that ~5 nm Al_2O_3 done by ALD is deposited on ~2.27 nm BN nanosheets. Fig. 2 shows the Raman spectra of the BN samples without and with Al_2O_3 layer, and the peaks are clearly observed at 1364.9 cm^{-1} and 1367.9 cm^{-1}, respectively. The blue-shift was caused by the compression which was introduced by the capped layer and the changes of bond in lattice structure.

Raman thermography was widely used to represent the thermal properties of 2D nano-materials, for their high sensitivity of frequency to temperature shift [30,31]. In process of rising temperature from 300 K to 500 K, Fig. 3 (a) and (b) show the temperature-dependent Raman spectra of BN samples without and with Al_2O_3 layer, respectively. Obviously, Raman phonon mode E_{2g} peaks exhibit a red-shift with increasing temperature, and form an approximate linear relation as shown in Fig. 3 (c) by $\omega = \omega_0 + \chi_T \Delta T$ [32], where ω_0 is the Raman mode frequency at room temperature, χ_T is the first-order temperature coefficient, and ΔT is the temperature difference with respect to room temperature. The measured χ_T value of the pure BN film sample approaches to $-0.02243\ cm^{-1}$/K, similar to previously reported value ($-0.022 \pm 0.003\ cm^{-1}$/K) [15], while the corresponding value of BN sample capped with Al_2O_3 layer is about $-0.06544\ cm^{-1}$/K, twice larger than the former. The shift can be account for the fact that the thermal expansion of the lattice changes the phonon energy. The higher slope makes a conclusion that Al_2O_3 capping layer reduces the thermal stability of pure BN, which accords with their thermal expansion coefficients reported in previous works: $-2.9 \times 10^{-6}\ K^{-1}$ for BN as well as $7.85 \times 10^{-6}\ K^{-1}$ for Al_2O_3 [33]. In general, the observed softening of the Raman mode with temperature origins from an anharmonicity, which is related to the anharmonic potential constant, the phonon occupation as well as the thermal expansion of the crystal [26]. However, the Raman shift method is also used to measure the thermal properties of suspended as well as substrate-supported/capping layer effects on nano-materials such as thin-films, nanoparticles, and individual CNTs [34–36].

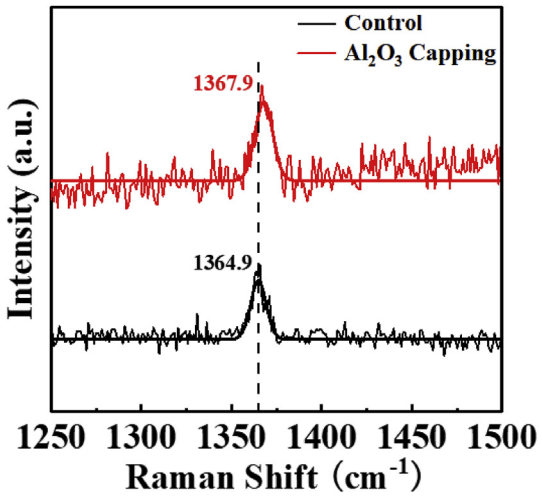

Fig. 2. Raman spectra of BN samples with and without Al_2O_3 capping layer on SiO_2/Si substrates.

In order to calculate the thermal conductivity, laser power-dependent Raman spectroscopy has been carried out for both samples in non-uniform range up to P_0. We use a confocal Raman microprobe equipped with a 514 nm laser for excitation and the maximum laser power P_0 was set as 2.5 mW measured at the exit of the microscope lens, in case to reduce the temperature change influences. It can be reduced to lower powers to avoid smashing up the thin BN layers and those are $0.5P_0$, $0.1P_0$, and $0.05P_0$, respectively, using an optical attenuator. Fig. 4 (a) and (b) display the room-temperature frequency information of the power-dependent Raman spectra of BN samples without and with Al_2O_3 capping layer, respectively, at several laser power points. Evidently, similar to the temperature-dependent Raman spectra above, Raman phonon mode E_{2g} peaks exhibit a red-shift with increasing laser power, and as shown in Fig. 4 (c), it is fitted by a linear equation $\Delta\omega = \chi_P \Delta P$, where χ_P is the first-order power coefficient and ΔP is the power difference value. The fitted slope χ_P related frequency with laser power of BN sample roughly equals to $-2.09774\ cm^{-1}$/mW, which is larger than the corresponding value ($-1.84962\ cm^{-1}$/

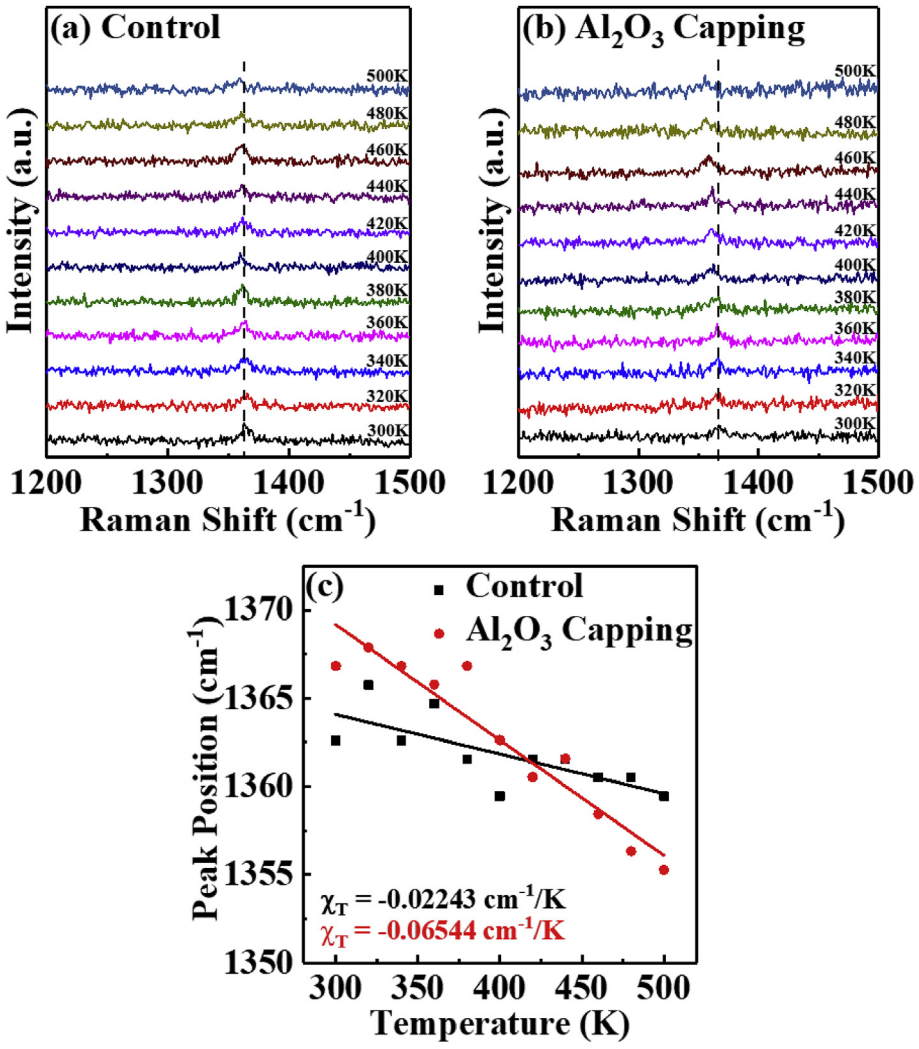

Fig. 3. Temperature-dependent Raman spectra of (a) BN and (b) Al_2O_3/BN samples on SiO_2/Si substrates in the range of 300–500 K, and (c) E_{2g} mode Raman peak position shift as a function of temperature including linear fits.

mW) of BN/Al_2O_3 sample. In power-dependent Raman experiments, the laser power will not be completely absorbed by BN sample, part of that reflected at air-BN, air-oxide(Al_2O_3), and BN-oxide(Al_2O_3) interfaces. So, a laser reduction factor f should be considered as f=(1-R)[1-exp(-αt)], where R is reflectance calculated by $R=[(n_1\text{-}n_2)/(n_1+n_2)]^2$, α is absorption coefficient, and t is thickness of film. Using refractive index $n_{air}=1$, $n_{BN}=2.20$ [22], $n_{oxide}=1.77$, reflectance can be calculated as $R_{air/BN}=14.06\%$, $R_{air/oxide}=7.73\%$, $R_{BN/oxide}=1.17\%$. Then, taking $\alpha_{BN}=7\times10^5 cm^{-1}$ and $t=2.27$ nm into account [13], we can obtain the laser reduction factors of BN samples without and with Al_2O_3 layer are equal to 0.126 and 0.134, respectively. The thermal conductivity k formula, initially used for single layer graphene (SLG), was expressed as k=($1/2\pi t$)($\Delta P/\Delta T$) [37], where ΔP and ΔT are the power and temperature difference values, respectively, and t is thickness of film. In this work, according to $\Delta\omega=\chi_T\Delta T$, the thermal conductivity formula can be adapted as $k=f(1/2\pi t)(\chi_T/\chi_P)$, where f is the laser reduction factor, χ_T and χ_P are the first-order temperature and power coefficients, respectively, as well as t is the thickness of film. Taking the related values calculated above into the equation, we can obtain that the thermal conductivity of BN without Al_2O_3 layer is about 94.51 W/mK. The result is similar to that of CVD-BN reported (100 ± 10 W/mK) [19], but lower than values of suspended BN nanosheets reported (222.3–250 W/mK) [15,18,38,39], due to the existence of interlayer (between sample and substrate) phonon scattering. Whereas, the thermal conductivity of BN with Al_2O_3 layer has enhanced up to 332.57 W/mK, much larger than the former, which demonstrates that the Al_2O_3 layer capped onto BN film profoundly improves thermal transport of materials. The enhancement of thermal conduction ability may put down to the interface charges existed at BN-Al_2O_3 interface, which give rise to the electron-phonon interactions. Besides, it also can be attributed to the compressive stress given by Al_2O_3 capping layer for the different thermal expansion coefficients, which changes the lattice structure and parameters. However, the intrinsic vibration properties of BN films weakly bonded to the SiO_2/Si substrates can be modulated by the substrate owing to the different thermal expansion coefficients between them. Thus, the temperature-dependent Raman spectroscopy of the samples in this work was less susceptible to the substrate effect, implying that the improved thermal coefficients of the BN films in Al_2O_3/BN/SiO_2/Si mainly results from the Al_2O_3 capping layer rather than other environment factors. On the other hand, it is the observation that the thermal conductivity is negligible in c-axis direction of FLBN compared to the in-plane value. Although the Al_2O_3 capping layer is thicker than previous BN nanosheets, we can rule out the possibility that the

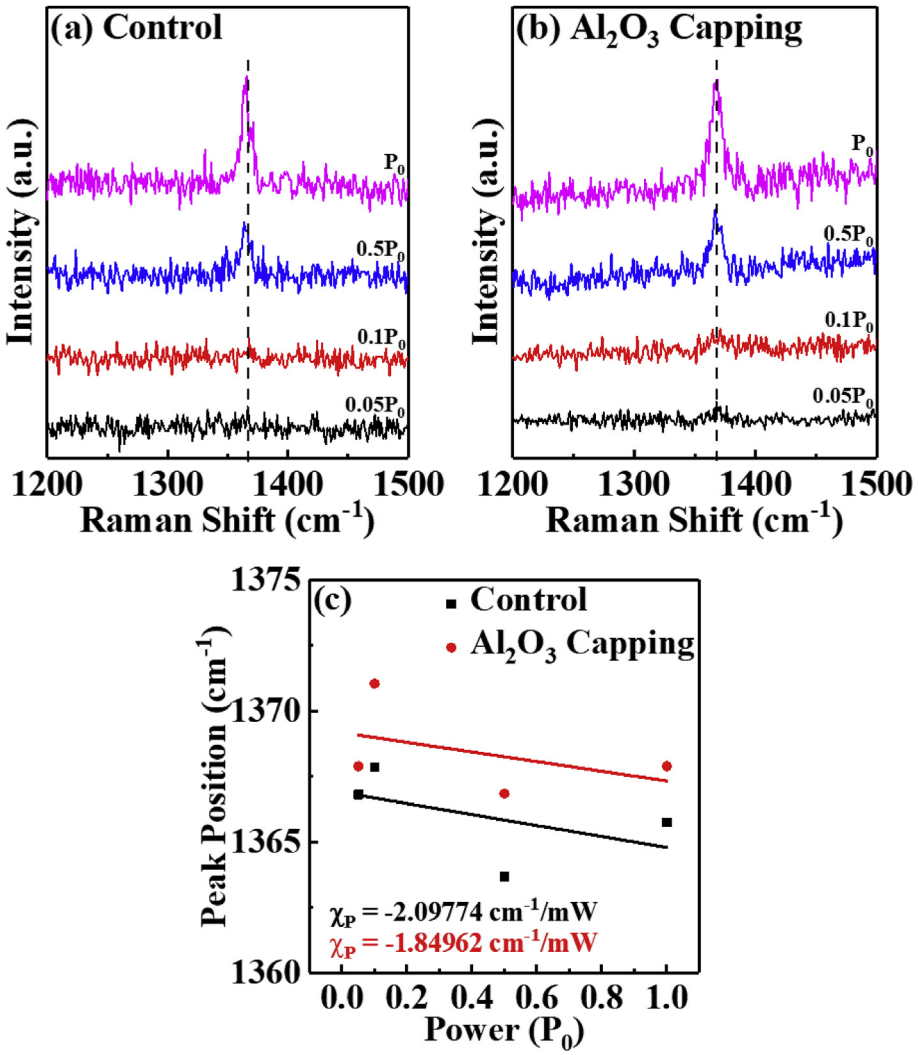

Fig. 4. Laser power-dependent Raman spectra of (a) BN and (b) Al_2O_3/BN samples on SiO_2/Si substrates in the range of $0.05P_0$ to P_0, and (c) E_{2g} mode Raman peak position shift as a function of power.

heat of Raman laser spot is mainly dissipated in out-plane direction through Al_2O_3. This is due to the interlayer coupling in few-layer BN, which results in the breaking of the phonon scattering selection rule in monolayer BN, thus reducing the relevant thermal conductivity values. The values converge to that of bulk hBN when the layer thickness approaches to 5 layers or more. In other words, monolayer or bilayers BN behave unexpected variation in peak position, but the phonon barely exists for FLBN thicker than 5 layers [22,38].

It is well known that the electrons give the main contribution to the thermal conductivity of strongly degenerate matter. From the Wiedemann–Franz law, the thermal conductivity can be written as [40]

$$k_e = \pi^2 T k_B^2 n_e / 3 m_e^* \nu_e, \quad (1)$$

where T is the temperature, k_B is the Boltzmann constant, n_e is the number density of electrons, m_e^* is the effective mass of electron and ν_e is the total effective electron collision frequency. The Cambridge Sequential Total Energy Package (CASTEP) based on density-functional theory (DFT) was used to simulate the influence of compressive strain given on band structure of BN film for electronic study [41]. We treat the ion-electron interactions via the generalized gradient approximation for the exchange and correlation potential by Perdew-Burk-Ernzerhof (PBE) [42], together with the projector augmented-wave method (PAW) [43]. For the structure optimization and total energy calculation, the value of plane-wave cut-off energy was 400 eV and the Brillouin zone was sampled by a Γ-centered k-point mesh generated via the Monkhorst–Pack method using a $4 \times 4 \times 1$ k mesh [44]. As the total energy changes finally converged to less than 10^{-4} eV/atom during the optimization, all the atoms are relaxed to their equilibrium positions. For each one, the force in the crystal is converged to 0.003 eV/nm, the stress is converged to 0.05 GPa, and the displacement is converged to 1×10^{-4} nm. Fig. 5 (a)~(d) exhibit the calculation results of band structure with compressive strain from 0% to 3% for few-layer BN, respectively. It indicates that with the increasing compressive strain, band structure occurs a great change, quantitatively expressed as the constantly shrinking band gap from 4.31 eV to 4.21 eV. Further analysis shows that the top of valence band stays in position while the bottom of conduction band turns lower at the Γ point, as shown in Fig. 5 (e). The effective mass of the charge carrier can be calculated using $m^* = \hbar^2 / \left(\frac{\partial^2 E}{\partial^2 k}\right)$, then the

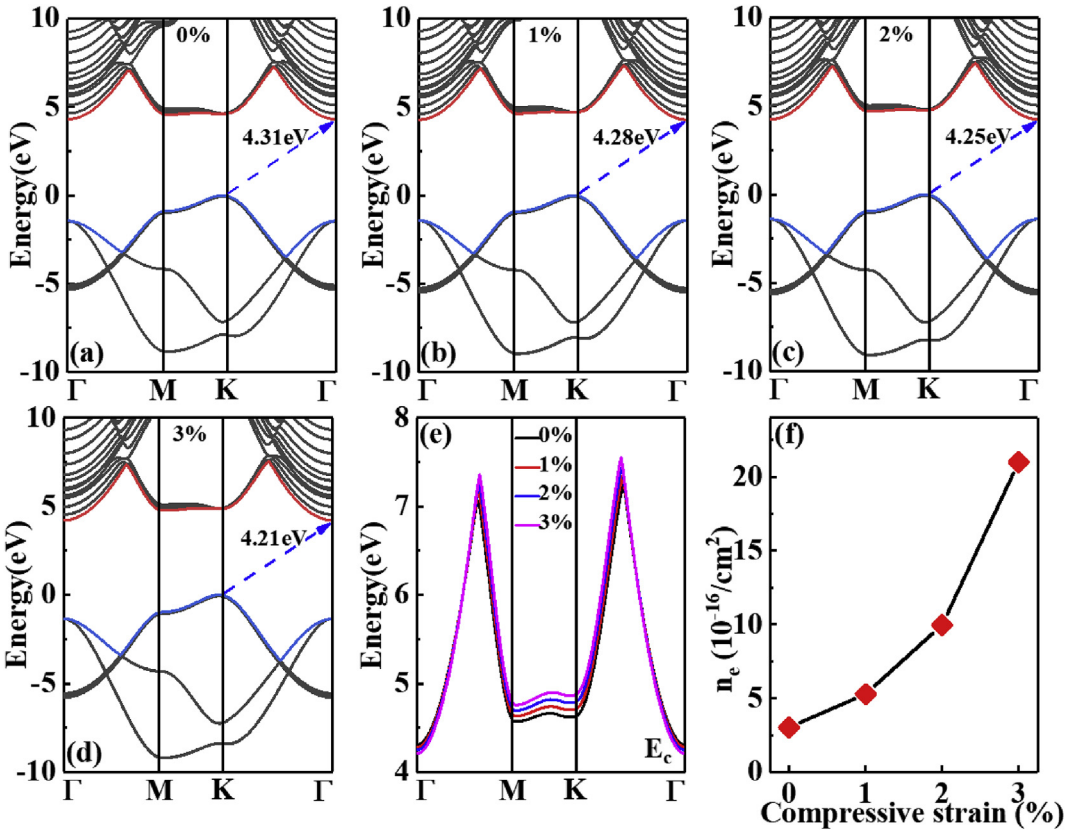

Fig. 5. Band structures for four-layers of BN structure at (a) 0%, (b) 1%, (c) 2%, and (d) 3% compressive strain. (e) The bottom of conduction band at different compressive strain percentages, and (f) the corresponding electron concentration with compressive strain.

electron concentration (n_e) can be estimated as

$$n_e = 2\left(\frac{k_B T}{2\pi\hbar^2}\right)^{3/2}(m_e m_h)^{3/4} exp(-E_g/2k_B T), \quad (2)$$

where k_B is Boltzmann constant, T is the temperature, $\hbar = h/(2\pi)$, h is Planck constant, m_e is mass of electron, m_h is mass of hole, and E_g is band gap. Fig. 5 (f) shows the corresponding measured electron concentration with increasing compressive strain. As a consequence of shrinking negative exponential factor E_g, n_e is on the rise, implying that the value of k is also enlarged, in line with the Raman spectroscopy results.

4. Conclusion

In summary, atomically thin BN film on SiO_2/Si substrates has been prepared by mechanically exfoliation method and capped with a ~5 nm Al_2O_3 capping layer by ALD to investigate the effects of the oxide on thermal properties, using the temperature-dependent and the polarized-laser power-dependent Raman spectroscopy measurements. As a result, the Raman peak position of E_{2g} vibration mode exists a blue-shift from 1364.9 cm^{-1} to 1367.9 cm^{-1}, the first order temperature coefficient is found increasing from $-0.02243\ cm^{-1}$/K to $-0.06544\ cm^{-1}$/K, as well as the room-temperature thermal conductivity of BN without and with Al_2O_3 layer is about 94.51 W/mK and 332.57 W/mK, respectively. The enhancement is mainly attributed to electron-phonon interaction and compressive stress at the interface between BN/Al_2O_3 heterostructure, which is due to the increasing electron concentration.

Acknowledgement

This work is supported by the National Key Research and Development Program of China (2017YFB0403000), China; National Science Fund for Distinguished Young Scholars (61725403), China; CAS Pioneer Hundred Talents Program, China; Guangdong Province Key Research and Development Plan (2019B010138002), China.

References

[1] C. Zhi, Y. Bando, C. Tang, H. Kuwahara, D. Golberg, Large-scale fabrication of boron nitride nanosheets and their utilization in polymeric composites with improved thermal and mechanical properties, Adv. Mater. 21 (2009) 2889–2893.
[2] A. Ambrosio, M. Tamagnone, K. Chaudhary, L.A. Jauregui, P. Kim, W.L. Wilson, F. Capasso, Selective excitation and imaging of ultraslow phonon polaritons in thin hexagonal boron nitride crystals, Light Sci. Appl. 7 (2018) 27.
[3] K. Watanabe, T. Taniguchi, H. Kanda, Direct-bandgap properties and evidence for ultraviolet lasing of hexagonal boron nitride single crystal, Nat. Mater. 3 (2004) 404.
[4] L. Ci, L. Song, C. Jin, D. Jariwala, D. Wu, Y. Li, A. Srivastava, Z.F. Wang, K. Storr, L. Balicas, F. Liu, P.M. Ajayan, Atomic layers of hybridized boron nitride and graphene domains, Nat. Mater. 9 (2010) 430.
[5] S.K. Jang, J. Youn, Y.J. Song, S. Lee, Synthesis and characterization of hexagonal boron nitride as a gate dielectric, Sci. Rep. 6 (2016) 30449.
[6] C.R. Dean, A.F. Young, I. Meric, C. Lee, L. Wang, S. Sorgenfrei, K. Watanabe, T. Taniguchi, P. Kim, K.L. Shepard, J. Hone, Boron nitride substrates for high-quality graphene electronics, Nat. Nanotechnol. 5 (2010) 722.
[7] I. Meric, C.R. Dean, N. Petrone, L. Wang, J. Hone, P. Kim, K.L. Shepard, Graphene field-effect transistors based on boron–nitride dielectrics, Proc. IEEE 101 (2013) 1609–1619.
[8] K.H. Lee, H.-J. Shin, J. Lee, I.-y. Lee, G.-H. Kim, J.-Y. Choi, S.-W. Kim, Large-scale synthesis of high-quality hexagonal boron nitride nanosheets for large-area graphene electronics, Nano Lett. 12 (2012) 714–718.
[9] K.K. Kim, A. Hsu, X. Jia, S.M. Kim, Y. Shi, M. Dresselhaus, T. Palacios, J. Kong, Synthesis and characterization of hexagonal boron nitride film as a dielectric

layer for graphene devices, ACS Nano 6 (2012) 8583–8590.
[10] M.P. Levendorf, C.-J. Kim, L. Brown, P.Y. Huang, R.W. Havener, D.A. Muller, J. Park, Graphene and boron nitride lateral heterostructures for atomically thin circuitry, Nature 488 (2012) 627.
[11] L. Britnell, R.V. Gorbachev, R. Jalil, B.D. Belle, F. Schedin, A. Mishchenko, T. Georgiou, M.I. Katsnelson, L. Eaves, S.V. Morozov, N.M.R. Peres, J. Leist, A.K. Geim, K.S. Novoselov, L.A. Ponomarenko, Field-effect tunneling transistor based on vertical graphene heterostructures, Science 335 (2012) 947–950.
[12] K. Watanabe, T. Taniguchi, T. Niiyama, K. Miya, M. Taniguchi, Far-ultraviolet plane-emission handheld device based on hexagonal boron nitride, Nat. Photon. 3 (2009) 591.
[13] J. Li, S. Majety, R. Dahal, W.P. Zhao, J.Y. Lin, H.X. Jiang, Dielectric strength, optical absorption, and deep ultraviolet detectors of hexagonal boron nitride epilayers, Appl. Phys. Lett. 101 (2012) 171112.
[14] M. Autore, P. Li, I. Dolado, F.J. Alfaro-Mozaz, R. Esteban, A. Atxabal, F. Casanova, L.E. Hueso, P. Alonso-González, J. Aizpurua, A.Y. Nikitin, S. Vélez, R. Hillenbrand, Boron nitride nanoresonators for phonon-enhanced molecular vibrational spectroscopy at the strong coupling limit, Light Sci. Appl. 7 (2018) 17172.
[15] L. Ziyuan, L. Chunru, C. Yang, High thermally conductive and electrically insulating 2D boron nitride nanosheet for efficient heat dissipation of high-power transistors, 2D Mater. 3 (2016), 041009.
[16] Z. Yan, G. Liu, J.M. Khan, A.A. Balandin, Graphene quilts for thermal management of high-power GaN transistors, Nat. Commun. 3 (2012) 827.
[17] L. Lindsay, D.A. Broido, Enhanced thermal conductivity and isotope effect in single-layer hexagonal boron nitride, Phys. Rev. B 84 (2011) 155421.
[18] I. Jo, M.T. Pettes, J. Kim, K. Watanabe, T. Taniguchi, Z. Yao, L. Shi, Thermal conductivity and phonon transport in suspended few-layer hexagonal boron nitride, Nano Lett. 13 (2013) 550–554.
[19] M.T. Alam, M.S. Bresnehan, J.A. Robinson, M.A. Haque, Thermal conductivity of ultra-thin chemical vapor deposited hexagonal boron nitride films, Appl. Phys. Lett. 104 (2014), 013113.
[20] W.-L. Song, P. Wang, L. Cao, A. Anderson, M.J. Meziani, A.J. Farr, Y.-P. Sun, Polymer/boron nitride nanocomposite materials for superior thermal transport performance, Angew. Chem. 124 (2012) 6604–6607.
[21] T. Park, H. Kim, M. Leem, W. Ahn, S. Choi, J. Kim, J. Uh, K. Kwon, S.-J. Jeong, S. Park, Y. Kim, H. Kim, Atomic layer deposition of Al2O3 on MoS2, WS2, WSe2, and h-BN: surface coverage and adsorption energy, RSC Adv. 7 (2017) 884–889.
[22] R.V. Gorbachev, I. Riaz, R.R. Nair, R. Jalil, L. Britnell, B.D. Belle, E.W. Hill, K.S. Novoselov, K. Watanabe, T. Taniguchi, A.K. Geim, P. Blake, Hunting for monolayer boron nitride: optical and Raman signatures, Small 7 (2011) 465–468.
[23] D. Pacilé, J.C. Meyer, Ç.Ö. Girit, A. Zettl, The two-dimensional phase of boron nitride: few-atomic-layer sheets and suspended membranes, Appl. Phys. Lett. 92 (2008) 133107.
[24] L. Zhu, F. Liu, H. Lin, J. Hu, Z. Yu, X. Wang, S. Fan, Angle-selective perfect absorption with two-dimensional materials, Light Sci. Appl. 5 (2016), e16052.
[25] H. Frostig, T. Bayer, Y.C. Eldar, Y. Silberberg, Revealing true coupling strengths in two-dimensional spectroscopy with sparsity-based signal recovery, Light Sci. Appl. 6 (2017), e17115.
[26] B. Fazio, P. Artoni, M. Antonia Iatì, C. D'Andrea, M.J. Lo Faro, S. Del Sorbo, S. Pirotta, P. Giuseppe Gucciardi, P. Musumeci, C. Salvatore Vasi, R. Saija, M. Galli, F. Priolo, A. Irrera, Strongly enhanced light trapping in a two-dimensional silicon nanowire random fractal array, Light Sci. Appl. 5 (2016), e16062.
[27] A.C. Ferrari, J.C. Meyer, V. Scardaci, C. Casiraghi, M. Lazzeri, F. Mauri, S. Piscanec, D. Jiang, K.S. Novoselov, S. Roth, A.K. Geim, Raman spectrum of graphene and graphene layers, Phys. Rev. Lett. 97 (2006) 187401.
[28] H. Li, Q. Zhang, C.C.R. Yap, B.K. Tay, T.H.T. Edwin, A. Olivier, D. Baillargeat, From bulk to monolayer MoS2: evolution of Raman scattering, Adv. Funct. Mater. 22 (2012) 1385–1390.
[29] Q. Cai, D. Scullion, A. Falin, K. Watanabe, T. Taniguchi, Y. Chen, E.J.G. Santos, L.H. Li, Raman signature and phonon dispersion of atomically thin boron nitride, Nanoscale 9 (2017) 3059–3067.
[30] I. Calizo, A.A. Balandin, W. Bao, F. Miao, C.N. Lau, Temperature dependence of the Raman spectra of graphene and graphene multilayers, Nano Lett. 7 (2007) 2645–2649.
[31] R. Yan, J.R. Simpson, S. Bertolazzi, J. Brivio, M. Watson, X. Wu, A. Kis, T. Luo, A.R. Hight Walker, H.G. Xing, Thermal conductivity of monolayer molybdenum disulfide obtained from temperature-dependent Raman spectroscopy, ACS Nano 8 (2014) 986–993.
[32] A.S. Pawbake, M.S. Pawar, S.R. Jadkar, D.J. Late, Large area chemical vapor deposition of monolayer transition metal dichalcogenides and their temperature dependent Raman spectroscopy studies, Nanoscale 8 (2016) 3008–3018.
[33] R.S. Pease, An X-ray study of boron nitride, Acta Crystallogr. 5 (1952) 356–361.
[34] V.D. Botcha, M. Zhang, K. Li, H. Gu, Z. Huang, J. Cai, Y. Lu, W. Yu, X. Liu, High-K substrate effect on thermal properties of 2D InSe few layer, J. Alloys Compd. 735 (2018) 594–599.
[35] V.D. Botcha, Y. Hong, Z. Huang, Z. Li, Q. Liu, J. Wu, Y. Lu, X. Liu, Growth and thermal properties of various In2Se3 nanostructures prepared by single step PVD technique, J. Alloys Compd. 773 (2019) 698–705.
[36] Q. Li, C. Liu, X. Wang, S. Fan, Measuring the thermal conductivity of individual carbon nanotubes by the Raman shift method, Nanotechnology 20 (2009) 145702.
[37] A.A. Balandin, S. Ghosh, W. Bao, I. Calizo, D. Teweldebrhan, F. Miao, C.N. Lau, Superior thermal conductivity of single-layer graphene, Nano Lett. 8 (2008) 902–907.
[38] H. Zhou, J. Zhu, Z. Liu, Z. Yan, X. Fan, J. Lin, G. Wang, Q. Yan, T. Yu, P.M. Ajayan, J.M.J.N.R. Tour, High thermal conductivity of suspended few-layer hexagonal boron nitride sheets, Nano Res. 7 (2014) 1232–1240.
[39] C. Wang, J. Guo, L. Dong, A. Aiyiti, X. Xu, B. Li, Superior thermal conductivity in suspended bilayer hexagonal boron nitride, Sci. Rep. 6 (2016) 25334.
[40] P.S. Shternin, D.G. Yakovlev, Electron thermal conductivity owing to collisions between degenerate electrons, Phys. Rev. D 74 (2006), 043004.
[41] M.D. Segall, J.D.L. Philip, M.J. Probert, C.J. Pickard, P.J. Hasnip, S.J. Clark, M.C. Payne, First-principles simulation: ideas, illustrations and the CASTEP code, J. Phys. Condens. Matter 14 (2002) 2717.
[42] J.P. Perdew, K. Burke, M. Ernzerhof, Generalized gradient approximation made simple, Phys. Rev. Lett. 77 (1996) 3865–3868.
[43] P.E. Blöchl, Projector augmented-wave method, Phys. Rev. B 50 (1994) 17953–17979.
[44] H.J. Monkhorst, J.D. Pack, Special points for Brillouin-zone integrations, Phys. Rev. B 13 (1976) 5188–5192.